

Date of publication xxxx 00, 0000, date of current version xxxx 00, 0000.

Digital Object Identifier 10.1109/ACCESS.2017.DOI

Red Blood Cell Segmentation with Overlapping Cell Separation and Classification from an Imbalanced Dataset

KORRANAT NARUENATTHANASET¹, THANARAT H. CHALIDABHONGSE^{2,3}, (Member, IEEE), DUANGDAO PALASUWAN⁴, NANTHEERA ANANTRASIRICHAJ⁵, (Member, IEEE), ATTAKORN PALASUWAN⁴,

¹Department of Computer Engineering, Chulalongkorn University, Bangkok, Thailand

²Department of Computer Engineering, Chulalongkorn University, Bangkok, Thailand (e-mail: thanarat.c@chula.ac.th)

³Research Group on Applied Digital Technology in Medicine (ATM), Chulalongkorn University

⁴Oxidation in Red Cell Disorders Research Unit, Chulalongkorn University, Bangkok, Thailand

⁵Visual Information Laboratory, University of Bristol, Bristol BS8 1UB, UK

Corresponding author: Thanarat H. Chalidabhongse (e-mail: thanarat.c@chula.ac.th).

This research is partially funded by Newton Mobility Grant and Ratchadaphiseksomphot Endowment Fund Chulalongkorn University.

ABSTRACT Automated red blood cell (RBC) classification on blood smear images helps hematologists to analyze RBC lab results in a reduced time and cost. However, overlapping cells can cause incorrect predicted results, and so they have to be separated into multiple single RBCs before classifying. To classify multiple classes with deep learning, imbalance problems are common in medical imaging because normal samples are always higher than rare disease samples. This paper presents a new method to segment and classify RBCs from blood smear images, specifically to tackle cell overlapping and data imbalance problems. Focusing on overlapping cell separation, our segmentation process first estimates ellipses to represent RBCs. The method detects the concave points and then finds the ellipses using directed ellipse fitting. The accuracy from 20 blood smear images was 0.889. Classification requires balanced training datasets. However, some RBC types are rare. The imbalance ratio of this dataset was 34.538 for 12 RBC classes from 20,875 individual RBC samples. The use of machine learning for RBC classification with an imbalanced dataset is hence more challenging than many other applications. We analyzed techniques to deal with this problem. The best accuracy and F1-score were 0.921 and 0.8679, respectively, using EfficientNet-B1 with augmentation. Experimental results showed that the weight balancing technique with augmentation had the potential to deal with imbalance problems by improving the F1-score on minority classes, while data augmentation significantly improved the overall classification performance.

INDEX TERMS Image classification, image segmentation, overlapping cells, red blood cell

I. INTRODUCTION

In a hospital, Red blood cell (RBC) morphology analysis is a subprocess in the Complete Blood Count (CBC) process. This analysis plays an essential role in diagnosing many diseases, caused by RBC disorders, such as anemia, thalassemia, sickle cell disease, etc. The analysis mainly focuses on the shape, size, color, inclusions, and arrangement of RBCs [1]. Generally, the normal RBC shape is round, biconcave, with a pale central pallor and of 6–8 μm diameter. A hematologist manually analyzes the blood cells under a light microscope

from blood smear slides. This manual inspection is a long process and also requires practices and experiences. Since recent computer vision and image processing in the medical imaging area can provide efficient tools, it can help hematologists to automatically and less subjectively analyze RBC images from a microscope in a reduced time and cost.

Most of the studies in the area of RBC images have been to classify RBCs, as in to identify the type of RBCs in the image. Normally, the image, captured from a microscope, contains many cells so it has to segment the cells before

the classification process. The studies in RBC classification have mostly used deep learning techniques, where state-of-the-art results in image classification have improved recently. However, there are still several challenges to achieve this goal. Since RBCs in the image may overlap with each other, it is hard to find the edge of the cell. In the manual process, the hematologist usually avoids selecting an area that has a lot of overlapping cells. But in some situations, especially in automated methods, it is difficult to avoid these areas because the cells stick together leading to incorrect predicted results. Thus, automated segmentation must be able to handle the overlapping cells so that it can cover the real situation. In addition, blood smear slides may not have the same environment, such as lighting, zoom scale, and camera.

Recently, deep convolutional neural network for object detection and semantic segmentation has begun to be used for RBC detection [2]–[6]. The benefits of these deep end-to-end methods are that, first, they allow training a possibly complex learning system represented by a single model, bypassing the intermediate layers usually found in traditional pipeline approach. Secondly, it is possible to design a model that performs well without deep knowledge about each sub-problem in the complex system. However, the end-to-end approach is infeasible option in some cases, for example, a huge amount of data is not available, the intermediate results are needed, as well as the computational resources are not available.

For this research, our goal is to develop the RBC segmentation and classification that require low computational complexity resources such as mobile phones and tablets so that we can apply to develop a mobile application for the hematologist training. Secondly, the application requires to have an interface that shows individual cell colored based on its type, for a real-time user interaction feature. By using end-to-end Deep Learning object detection or instance segmentation would not be feasible to serve this purpose well comparing to the very efficient and accurate traditional low-level computer vision approach we proposed in this paper.

Although deep learning has shown remarkable results in computer vision, these approaches still need lots of data to achieve a good outcome. Nevertheless, RBC datasets are difficult to collect because some RBC types can only be found in specific diseases, and these may only be found in specific geographic regions. Accordingly, each dataset usually has an imbalance problem. Moreover, even then different specialists might give different results, depending on their expertise, and so shifts the analytical balance towards being subjective.

This paper presents a new framework for RBC segmentation using ellipse fitting and classification via the use of EfficientNet [7]. The main contributions of the paper are: (i) a new method to separate the overlapping cells based on the concave points of the border of RBCs, and (ii) RBC classification with analysis of imbalanced datasets using data augmentation, weight normalization, upsampling, and focal loss [8] on multi-class classification.

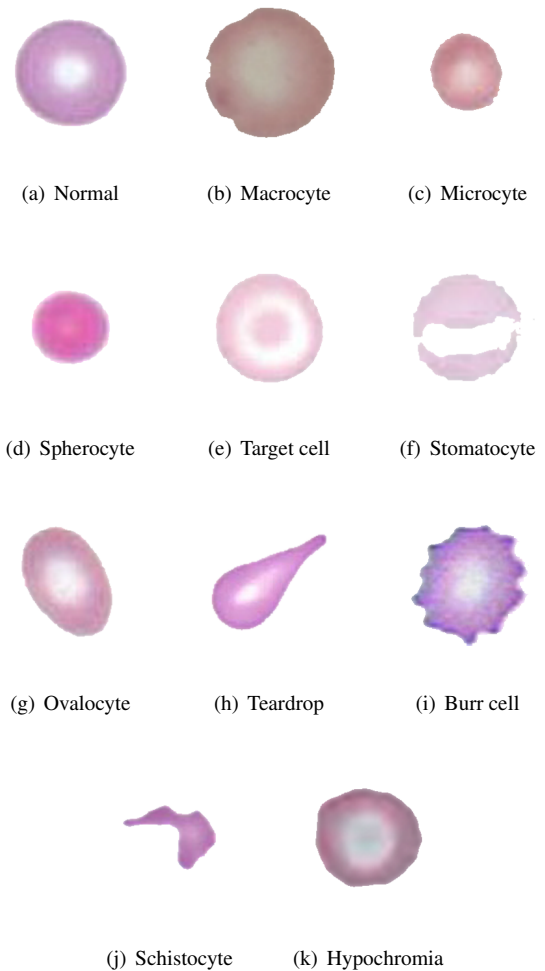


FIGURE 1. Different types of RBCs

II. TOTAL RBC COUNTS AND THE AUTOMATED METHODS

Blood smear image studies via computer vision areas usually target a specific cell type, such as white blood cell, RBC, and platelet [9]. The automated counting and classification of RBCs can be used in CBC, or in specific disease diagnoses, such as malaria, leukemia, and anemia. Counting of each abnormal RBC type, as a marker of disease and the level of critical illness, is normally performed by a hematologist. In this section, previous RBC studies are reviewed.

A. DIFFERENT RBC TYPES

The 11 RBC types focused on in this study as shown in figure 1. As observed from a blood smear slide under a microscope, normal RBCs are a red circle with a white pale circle in the middle (the central pallor), and these are the main cells found in the serum, while the other abnormal types are clearly different from normal RBCs in shape, size, color, inclusion, and arrangement [1]. Each type of abnormal RBC can be found in various types of diseases. For example,

in figure 1(b,c) the RBCs are bigger and smaller than the normal, respectively, while in Figure 1(d-f, k) they can be distinguished by observing their central pallor, and in Figure 1(g-i) they differ in the shape of the cells. Figure 1(j) shows a fragmented RBC. Note that inclusion RBCs, which are RBCs with dark dots inside, such as malaria parasite, are not focused on this study. Although, a single RBC might contain more than one characteristic type, such as Oval + Macrocyte or Hypochromia + Macrocyte, our classification studies is a multi-class classification, which each RBC has only one class.

B. SEGMENTATION OF CELLS

Automated RBC counting first focused on the number of RBCs in general, and then the precise shape extraction was focused on for use in subsequent classification steps. The automated process usually starts with converting the color image of blood smear images to a greyscale. Then, pre-processing is performed to improve the contrast and reduce the noise. Next, a segmentation step is applied followed by morphology operation to extract the RBC contours, with a difference method being used in the segmentation step. To identify a number of RBCs, circle Hough transformation was used, since this works well for circular shapes similar to that of RBCs [10], [11]. To extract the precise RBC shape, Otsu thresholding [12]–[20] was used in many studies, since it has been shown to strongly contrast between the RBC area and the background. For edge detection, Canny edge detection [21]–[23] and Sobel edge detection [24] have been used. Other studies have used other methods, such as Dijkstra's shortest path on the RBC border [25], ring shape dilation to identify the RBCs [26], and Watershed [27], [28], while an active appearance model on sliding windows [29], K-means [30], and histogram equalization [31] have also been used. The most recent studies have used a fully convolutional neural network (FCN) [32], FCN-Alexnet [33], U-net [34], and deformable U-net [35].

The segmentation can contain overlapping cells. To classify RBCs mostly requires separating them into single cells to compute their features or feed into a deep learning model. In addition, a step after their segmentation was included to separate overlapping cells, where the Circle Hough transformation was used to estimate RBCs in contour [11], [28]. Most studies have previously identified a number of RBCs in contour and then segmented the area of each cell. Distance transformation was used to find the peak spot as markers of RBCs, and then Watershed [19] or a random walk method [36] was applied. The area in a contour has been used to determine the number of RBCs [16], and then K-means was used on the pixel coordinates. In addition, purpose overlapping cell separation using ellipse adjustment with concave point finding has been used [37].

From these previous studies, several methods that extract RBCs from the background have been found to give good results because RBCs usually have a high contrast. However, it difficult to find the best algorithm to separate cells that

are connected to each other, because overlapping cells can have complex shapes. The watershed method can give good results on when separating overlapping cells that have a space between their centers, while ellipse adjustment needs a concave area between the cells. In addition, the FCN methods are good at segmenting the cells, due to the quality and number of datasets and labels, but they cannot separate overlapping cells, since they might not be able to count or have post-processing techniques.

C. CLASSIFICATION OF RBC TYPES

The classification of RBCs is firstly based on manual features, such as circularity, color average, diameter, area, etc. The features have been used in rule-based methods [12], [13], [18], [22], [38], K-nearest neighbor [28], and artificial neural network (ANN) [14], [30], [15], [31], [39], [40]. After that, convolutional neural networks (CNN) [19], [32], [34], [36], [41]–[46] have been used instead to auto-generate features due to the better computing power available nowadays, and they can be extended to encompass more classes of RBCs. In recent classification studies, CNN classifiers have been used with more layers and new techniques. Durant et al. [42] used DenseNet, which has more than 150 layers, to predict 10 RBC types. Focal loss was used to classify three RBC types from an imbalanced dataset [11].

For end-to-end CNN approach, a U-net [2], [3] have been used to perform both segmentation and classification in a single model. [4] purposed multi-label detection using a Faster R-CNN with ResNet was used to detect six types of RBCs with touching and overlapping cells while [5] used YOLOv3 [6] to detect RBCs, WBCs, and platelets.

From the results in each study, the most updated trend is based on deep learning where the performance of the outcome mostly depends on the size and quality of the dataset that was used. Every previous study has used their dataset to train and validate the result, but this makes it hard to compare them. Moreover, each dataset will still have small amounts of data, because of the data collection is mostly done in a hospital, which is a more difficult processes than general in a general image dataset collection. For multi-class classification, some RBC types are rare and hard to find, and so the dataset may have an imbalance problem.

To classify such minority classes, imbalance handling techniques can help the classification model to be less biased towards the majority classes. Oversampling and undersampling are common techniques used in the data level analysis to deal with the imbalance problem. Imbalance handling techniques on various data types at the data and algorithm levels have been reviewed [47], and shown that oversampling outperforms undersampling in most cases. Focal loss [8] is modified from the cross-entropy loss that helps the model to train on hard miss-classified samples and to focus less on well-classified samples.

III. PROPOSED METHODS

In this section, the proposed method is outlined, starting from normalizing the images and extracting an individual cell from blood smear images to identifying the type of each RBC, which is described by dividing it into the four main steps of: (i) RBC color normalization, (ii) overlapping cell separation, (iii) RBC contour extraction, and (iv) RBC classification. The overall process is summarized in Figure 2.

A. COLOR NORMALIZATION

In the data collection process, collectors might have different environments, such as camera settings, microscope light levels, blood smear slide preparation, etc. The collectors also might collect multiple blood smear slides of a single RBC type at a time, making each type have its own color space, as shown in Figure 2. Although, hematologists can disregard the difference in color space from expertise, the model can be biased from the different color spaces during the training process instead of the characteristics of that type.

In this step, the backgrounds were extracted and the three overall average background values of the RGB channels (R_{avg} , G_{avg} , B_{avg}) were found for all the blood smear images. Before training and predicting the results, the different values of the three average background values of the target image k (r_{avg}^k , g_{avg}^k , b_{avg}^k) and the overall averages values were added to all the pixels of the target image. The normalization equation of pixel (i, j) for image k is shown in Eq. 1. Although, only the normalized images were used for improving the classification results, a huge improvement in the normalization accuracy was found (as shown in the results section).

$$\begin{aligned} r_{i,j}^k &= r_{i,j}^k + (R_{avg} - r_{avg}^k) \\ g_{i,j}^k &= g_{i,j}^k + (G_{avg} - g_{avg}^k) \\ b_{i,j}^k &= b_{i,j}^k + (B_{avg} - b_{avg}^k) \end{aligned} \quad (1)$$

B. RBC CONTOUR EXTRACTION

To extract the RBC contours from blood smear images, the color RBC image was first converted to a grayscale image using the green channel image from the RGB image, as this has more contrast than other channels, (Figure 3). Then CLAHE (Contrast Limited Adaptive Histogram Equalization), a histogram equalization program that is applied to a small uniformly divided region, was used to enhance the RBC regions out of the background. Finally, the Otsu threshold and contour findings were used to extract cell regions. The overall process is shown in Figure 4.

C. OVERLAPPING CELL SEPARATION

In manual RBC analysis, hematologists typically avoid selecting an area in a blood smear slide that has overlapping cells to evaluate the result. This is because it is simple to count and identify the type of RBC when their border is not hidden behind other cells. To separate the overlapping RBCs, the most reliable methods are based on distance transforming

and ellipse fitting. The distance transform approach is used to find the peak spots furthest from the border. The peak spots are then used to identify a unique cell by several techniques, such as the random walk method and watershed transform, and the area of each cell was found. However, although the distance transform works effectively for a circular shape and a small group of overlapping cells, the peak area may coexist making it difficult to specify a certain amount. The ellipse fitting method uses the edge of the RBC to approximate as an ellipse which identifies the area of RBC.

The method presented herein is based on ellipse fitting and the overall process was divided into four steps, as detailed below.

1) Concave point finding

In each point (coordinate) in the RBC contour, (x_i, y_i) , k middle points were calculated by finding the center of the distance between k pairs of contour points near the point. If all k points are outside the contour, the point is considered as a concave point. However, when more than one concave point can be found in a wide curve, only one concave point was selected by averaging all near concave points. The concave points function, $f(x)$, was calculated using Eqs. (2) and (3):

$$f(x_i, y_i) = \prod_{j=1}^k g\left(\frac{x_{i-j} + x_{i+j}}{2}, \frac{y_{i-j} + y_{i+j}}{2}\right) \quad (2)$$

$$g(x) = \begin{cases} 1, (x, y) & \text{is outside a contour,} \\ 0, (x, y) & \text{is inside a contour} \end{cases} \quad (3)$$

2) Ellipse estimation

If the contour has more than one concave point, curves between the two concave points were used to approximate an ellipse shape by direct ellipse fitting [48], based on the least-square method. The direct ellipse fitting is recommended instead of the original [49], which gives an approximate ellipse that does not relate to the curve in some conditions. The direct ellipse fitting is constrained by ensuring the discriminant $4ac - b^2 = 0$ for the ellipse equation, as shown in Eq. (4).

$$ax^2 + bxy + cy^2 + dx + ey + f = 0 \quad (4)$$

3) Ellipse verification

After finding all the ellipses in each contour, the ellipses were sorted by area in descending order. Then, each ellipse was verified to be in the RBC contour by meeting two simple conditions of (i) 80% of the ellipse area is in the contour and (ii) 20% in the remaining area in the contour is not in any previous ellipses.

4) Two curve ellipse estimation

In highly overlapping RBCs, more than two cells overlap each other and so the curves might not be able to restore the correct ellipse shape of each RBC. If there are more than two ellipses that do not pass the conditions, then the two curves were concatenated and used to estimate an ellipse of the remaining cell.

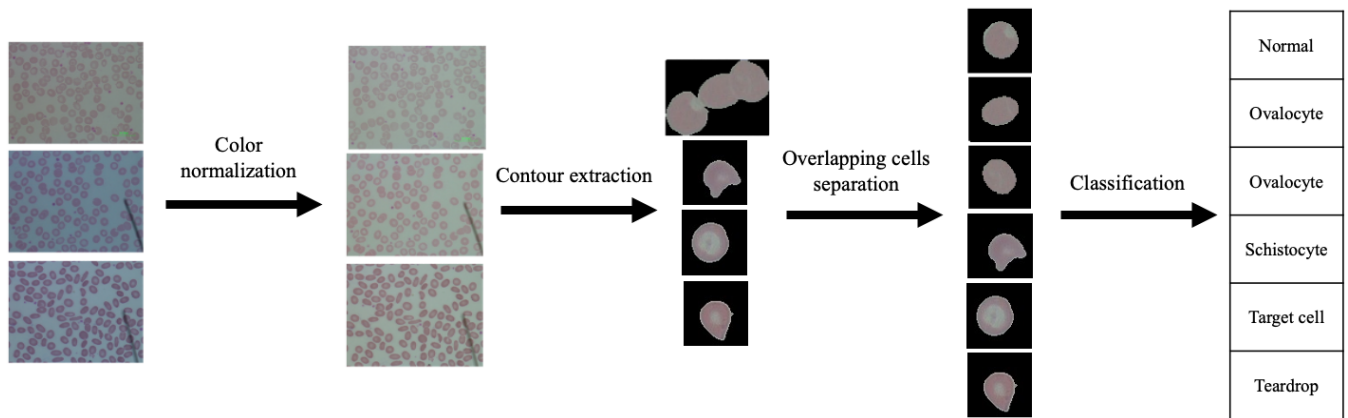


FIGURE 2. The pipeline of proposed method

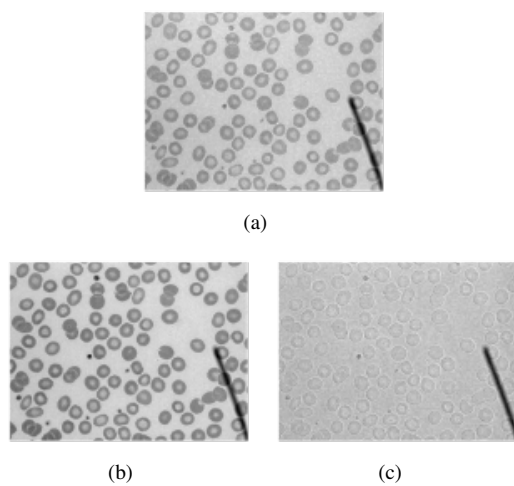


FIGURE 3. The RGB channels: (a) red channel image, (b) green channel image, and (c) blue channel image

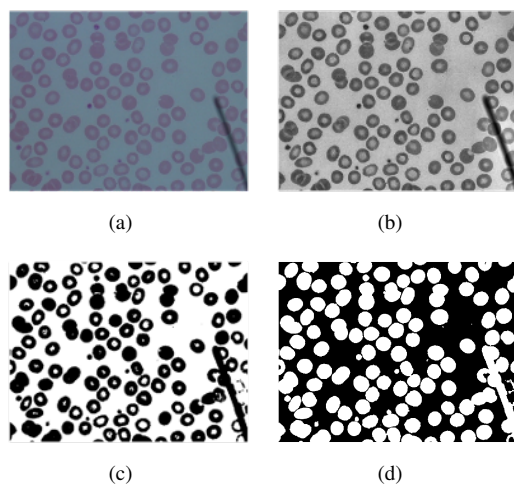


FIGURE 4. The (a) original image, (b) CLAHE image, (c) threshold image, and (d) contour image

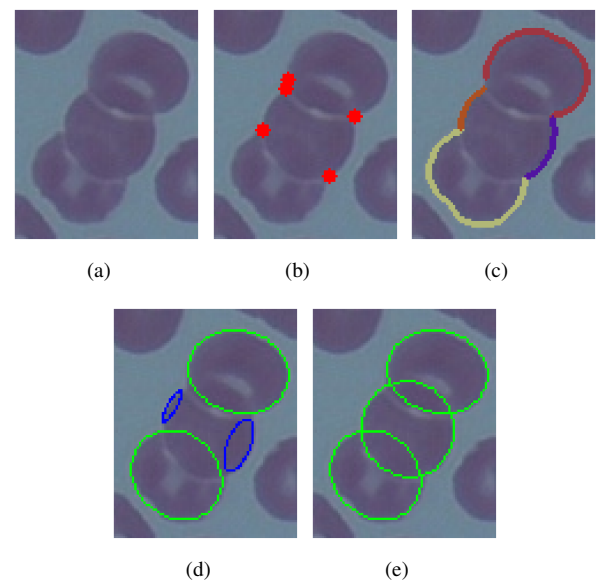


FIGURE 5. Steps in the overlapping cell separation: (a-c) two curves are concatenated and used to estimate an ellipse of the remaining cell. (d) The two blue ellipses show an incorrect cell estimation, while (e) shows the correct cell estimation after ellipse fitting with two curves.

D. RBC CLASSIFICATION

In this step, single contour images were created to feed the deep learning model. The dataset had 12 classes of RBCs: 11 RBC types and an uncategorized class, which is another type of RBC. The dataset was labeled by specialists in hematology. The numbers of RBCs in each class are shown in Table 1, while Figure 1 shows images of each type of RBC. The dataset is highly imbalanced because some classes are rare, such as the Teardrop, Sickle cell, and Uncategorized types.

1) EfficientNet

For classification, the pretrained EfficientNet model [7] was used as it showed a remarkable level of accuracy and better performance than the older models. It was designed by

carefully balancing the network depth, width, and resolution. The model has eight different sizes: EfficientNet-B0 to EfficientNet-B7. In the results section, the EfficientNet-B0 to EfficientNet-B4 were observed with a five-fold cross validation using 80% and 20% for training and testing, respectively. Moreover, we used data augmentation and weight initialization to observe which technique could overcome the class imbalance problem. Only random flips and rotates were used for data augmentation because the RBC classes are sensitive to size and color, such as Normal Macrocytes and Microcytes are different in size.

To evaluate the performance, accuracy is commonly used for image classification. For the imbalanced dataset, the accuracy is insufficient, as it can be dominated by the majority classes. However, many metrics have been used to describe an imbalanced dataset [47], and the F1-score was used in this study. This is a well-known metric that balances precision and recall by harmonic means that is sensitive to the minority classes.

2) Imbalance handling techniques

Further analysis on the imbalanced dataset was then performed. An imbalanced dataset is a common problem in biomedical datasets. Our RBC dataset was highly imbalanced with a 34.538 imbalance ratio (calculated from highest sample class/lowest sample class) for the 12 RBC classes from a total of 20,875 RBCs. In the training step, the model can be overcome by high sample classes with less focus on the low sample classes. Thus, the weight balancing, up sampling, and focal loss were investigated in this study.

For weight balancing, normally, every RBC class has the same weight, 1.0. However, the weight balancing helps a model balance learning gradients in the backpropagation step between high sample classes and low sample class, by giving a high weight to low sample classes and a low weight to high sample classes. In this study, each class was weighted as $\frac{1}{f}$, $\frac{1}{\sqrt{f}}$, and $\frac{1}{\sqrt[3]{f}}$ as weights 1, 2, and 3, respectively, where f is the amount of samples in that class.

The up sampling makes every RBC class have the same amount of samples by replicating its own data. This helps the trained model to not be overcome by high sample classes. In this case, every class replicates itself to match the normal class.

Focal loss is used to help the model focus on the high loss and reduce the loss near 0. It was used in the object detection task, which is highly imbalanced between objects and nonobject classes. We investigated if multi-class classification could help in an imbalanced multi-classification. As shown in Eq. 5, focal loss has an added term from the cross entropy loss, which reduces the loss when the predicted probability result is close to the known truth by the γ hyperparameter.

$$FL(p_t) = -(1 - p_t)^\gamma \log(p_t) \quad (5)$$

TABLE 1. Total number of each RBC class in the dataset

| RBC Class | Total number of RBCs |
|---------------|----------------------|
| Normal | 6,286 |
| Macrocyte | 687 |
| Microcyte | 459 |
| Spherocyte | 3,445 |
| Target cell | 2,703 |
| Stomatocyte | 1,991 |
| Ovalocyte | 2,137 |
| Teardrop | 305 |
| Burr cell | 783 |
| Schistocyte | 861 |
| Hypochromia | 1,036 |
| Uncategorised | 182 |
| Total | 20,875 |

TABLE 2. Overlapping cells separation result

| Contour | Correct | Incorrect (Concave) | Incorrect (Fitting) | Total |
|---------|---------|---------------------|---------------------|-------|
| 2 RBCs | 185 | 18 | 4 | 207 |
| 3 RBCs | 38 | 2 | 1 | 41 |
| >3 RBCs | 23 | 2 | 4 | 29 |
| Total | 246 | 22 | 9 | 277 |

IV. IMPLEMENTATIONS

The blood smear image size in our dataset was $640 * 480$ pixels. For the overlapping cells separation step, the k value was 8. The RBC contours were cropped and put on a blank $72 * 72$ image, which is big enough to contain the largest cell.

For classification, the contour images were scaled to $224 * 224$, which is the input size of EfficientNet model. The models were trained with pretrained parameters. The learning rate was 0.001 with a 0.1 learning decay rate in every 15 epochs, and a total of 100 epochs.

V. RESULTS

In this section, the overlapping cells separation and RBC classification results are provided and analyzed.

A. OVERLAPPING CELL SEPARATION

To evaluate the separation of the overlapping cells, we manually counted the overlapping contours that did not contain a cell on the border of the images and other artifacts, such as platelets, white blood cells, or microscope tools in the images. A total of 277 contours were found in 20 blood smear images, with an overall accuracy of 0.889. Most of the contours were two RBCs touching or overlapping with each other. The error in this method was mostly found on contours that had only one concave point. The results are summarized in Table 2, while blood smear images after segmentation are shown in Figure 6.

B. RBC CLASSIFICATION

In the first step, we investigated the different model sizes, EfficientNet-B0 to B4, with and without augmentation. The results (Table 3) show that EfficientNet-B1 with augmentation had the highest accuracy and F1-score. Thus, increasing the model size did not significantly improve the performance,

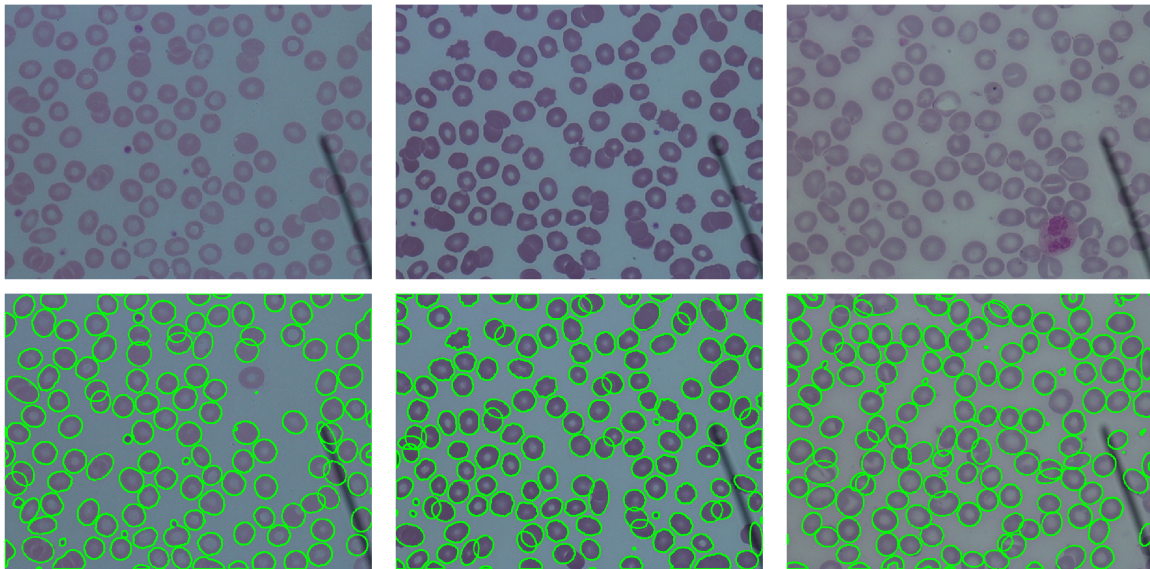


FIGURE 6. Segmentation results

TABLE 3. RBC classification results

| Model | Accuracy | F1-score |
|----------------------------|---------------|---------------|
| EfficientNet-B0 | 0.8821 | 0.8378 |
| EfficientNet-B1 | 0.8823 | 0.8426 |
| EfficientNet-B2 | 0.8842 | 0.8399 |
| EfficientNet-B3 | 0.8819 | 0.8423 |
| EfficientNet-B4 | 0.8830 | 0.8405 |
| EfficientNet-B0-aug | 0.8996 | 0.8639 |
| EfficientNet-B1-aug | 0.9021 | 0.8679 |
| EfficientNet-B2-aug | 0.8988 | 0.8636 |
| EfficientNet-B3-aug | 0.9001 | 0.8642 |
| EfficientNet-B4-aug | 0.8990 | 0.8668 |

and the limiting factor was the sample size of the dataset. Increasing the model size can then lead to an overfitting problem. Therefore, imbalance handling techniques were investigated, including weight balancing, up sampling, and focal loss, using EfficientNet-B1 as the baseline.

The overall training accuracy and F1-score of EfficientNet-B1 with imbalance handling techniques are summarized in Table 4. However, the baseline model with augmentation still had the highest accuracy and F1-score, followed by AugWeight3 (augmentation and $\frac{1}{\sqrt{T}}$ weight). Up (Up sampling) showed a slightly lower result from the baseline while AugUp (Augmentation with up sampling) showed slightly better results. Augmentation with focal loss (AugFocal0.5-AugFocal3.0) resulted in a decreasing accuracy and F1-score with increasing γ hyperparameter values.

Table 5 summarizes the F1-score in each class. The results revealed that Aug improved all class F1-scores from the baseline. Weight - Weight3 and AugWeight - AugWeight3 showed similar results compared to the baseline and Aug, respectively. AugWeight3 had six classes of RBCs with a better F1-score than Aug, which implied that an extremely different weight might not give an accurate result. AugUp

TABLE 4. Accuracy and F1-Score of our proposed EfficientNet-B1 with various data imbalance handling techniques

| Model | Accuracy | F1-score |
|-------------|---------------|---------------|
| Baseline | 0.8823 | 0.8426 |
| Aug | 0.9021 | 0.8679 |
| Weight | 0.8752 | 0.8374 |
| Weight2 | 0.8808 | 0.8435 |
| Weight3 | 0.8820 | 0.8410 |
| AugWeight | 0.8698 | 0.8344 |
| AugWeight2 | 0.8954 | 0.8630 |
| AugWeight3 | 0.8981 | 0.8672 |
| Up | 0.8772 | 0.8403 |
| AugUp | 0.8877 | 0.8591 |
| AugFocal0.5 | 0.8947 | 0.8523 |
| AugFocal1.0 | 0.8932 | 0.8510 |
| AugFocal1.5 | 0.8926 | 0.8543 |
| AugFocal2.0 | 0.8900 | 0.8480 |
| AugFocal2.5 | 0.8884 | 0.8486 |
| AugFocal3.0 | 0.8877 | 0.8488 |

had three RBC classes that were better than Aug with a huge improvement in the recognition of the Teardrop and Uncategorized types of RBCs. The focal loss was decreased when increasing the γ hyperparameter in all RBC classes.

In summary, the difference between this dataset and general datasets in the RBC classification problem are the dataset is imbalanced and RBC classes have many similar characteristics. Almost all classes are circular in shape, with only a few characteristics that are different, such as their size, shape, and color. The best result was obtained with the EfficientNet-B1 with augmentation.

Further analysis on an imbalanced dataset, weight balancing, and focal loss were examined for their effect on the loss function. Weight balancing helped to improve the low sample classes with less focus on the high sample classes. Otherwise, focal loss showed a decreased performance for this dataset

TABLE 5. F1-score of classifying RBCs classes using EfficientNet-B1 with data imbalance handling techniques

| Techniques | Normal | Macro | Micro | Spher | Target | Stoma | Ovalo | Tear | Burr | Schis | Uncat | Hypo |
|-------------|--------------|--------------|--------------|--------------|--------------|--------------|--------------|--------------|--------------|--------------|--------------|--------------|
| Baseline | 88.11 | 81.76 | 65.43 | 93.11 | 93.47 | 89.96 | 88.99 | 81.88 | 85.67 | 81.26 | 84.66 | 76.84 |
| Aug | 90.23 | 84.87 | 68.50 | 94.56 | 94.08 | 91.68 | 91.28 | 88.40 | 87.83 | 85.28 | 84.99 | 79.80 |
| Weight | 87.19 | 81.31 | 66.75 | 92.79 | 92.56 | 88.79 | 88.66 | 80.60 | 86.58 | 80.90 | 83.23 | 75.49 |
| Weight2 | 87.63 | 83.08 | 64.17 | 93.31 | 93.19 | 89.67 | 89.42 | 82.00 | 86.54 | 80.52 | 86.04 | 76.64 |
| Weight3 | 88.04 | 82.05 | 64.39 | 93.12 | 93.33 | 90.51 | 89.47 | 82.58 | 84.95 | 81.78 | 83.33 | 75.68 |
| AugWeight | 85.00 | 79.19 | 62.10 | 92.95 | 93.48 | 90.20 | 90.25 | 86.85 | 86.14 | 83.64 | 75.27 | 76.26 |
| AugWeight2 | 89.00 | 82.67 | 68.88 | 94.23 | 94.22 | 91.69 | 90.89 | 87.38 | 87.53 | 84.41 | 84.85 | 79.91 |
| AugWeight3 | 89.43 | 82.82 | 67.98 | 94.07 | 94.26 | 91.83 | 91.18 | 89.36 | 88.14 | 85.52 | 86.26 | 79.74 |
| Up | 87.87 | 79.46 | 60.36 | 92.86 | 93.36 | 88.67 | 89.10 | 86.44 | 82.28 | 80.98 | 90.14 | 76.81 |
| AugUp | 88.74 | 79.34 | 65.19 | 93.85 | 94.17 | 88.73 | 90.47 | 92.44 | 84.18 | 82.94 | 92.96 | 77.94 |
| AugFocal0.5 | 89.28 | 83.37 | 63.89 | 93.94 | 94.30 | 91.62 | 91.12 | 85.91 | 87.36 | 82.93 | 80.47 | 78.52 |
| AugFocal1.0 | 89.25 | 82.37 | 65.29 | 94.09 | 93.99 | 91.01 | 90.67 | 83.46 | 87.38 | 83.83 | 82.05 | 77.77 |
| AugFocal1.5 | 88.89 | 83.10 | 66.48 | 93.68 | 94.24 | 91.01 | 91.14 | 85.32 | 87.34 | 83.43 | 82.64 | 77.88 |
| AugFocal2.0 | 88.73 | 82.50 | 66.89 | 93.95 | 93.72 | 91.12 | 90.86 | 85.38 | 86.74 | 82.01 | 79.00 | 76.69 |
| AugFocal2.5 | 88.37 | 82.72 | 67.53 | 93.66 | 94.01 | 90.15 | 91.18 | 84.90 | 85.83 | 83.12 | 80.38 | 76.49 |
| AugFocal3.0 | 88.34 | 81.99 | 66.35 | 93.71 | 93.55 | 90.14 | 90.48 | 83.76 | 87.41 | 82.15 | 82.38 | 78.25 |

TABLE 6. Accuracy and F1-score of EfficientNet-B1 with different normalization techniques

| Model | Accuracy | F1-score |
|----------------|---------------|---------------|
| AugUnnormalize | 0.6325 | 0.4241 |
| AugBlackbg | 0.9021 | 0.8679 |
| AugWhitebg | 0.8977 | 0.8634 |
| AugGraybg | 0.8969 | 0.8603 |
| AugAVGbg | 0.8979 | 0.8626 |

because it focused on a high value loss, but since the different RBC classes were almost similar in shape the loss was almost entirely in the middle, which is ignored. Up sampling was performed at the data level, similar to augmentation. This technique seemed to work best for unique shape classes, which were the teardrop cell and uncategorized classes.

The analysis with a normalization step (Table 6) revealed a huge improvement compared to augmentation with an unnormalized image. We also trained the model with the different background colors of black, white, grey, and the average background color, where the black background gave the best result, slightly higher than the others.

Recently, [3] reported the results of using SVM and TabNet to classify the RBCs into 11 classes on the same dataset as used in this paper. They employed the SMOTE technique with cost-sensitive learning to handle the imbalanced dataset. The evaluation was done using F2-Score and the results show that the SVM outperforms the TabNet with 78.2% and 73.0% respectively. To compare with their work, we employed our methods, EfficientNet-B1 with augmentation, to classify 11 and 12 classes of RBCs on the same dataset. Our approach yields 88.62% and 87.91% F2-Score respectively.

C. COMPARISON ON THE YALE'S RBC DATASET

Since each of researchers usually has their own datasets which are different in the number of classes and the number of samples, thus the method comparison is quite not straightforward. However, we found an available RBC dataset used in Durant et.al. [42] provided by the Yale University School of Medicine. Their dataset contains 3,737 labeled RBCs with

10 classes including the overlapping cells. Durant et.al. used DenseNet [50] which has more than 150 layers. The reported accuracy was 0.9692 on the test set.

To make a fair comparison, we employed our proposed method based on the EfficientNet-B1 without the overlapping cell separation. We also used five-fold cross validation for training because we do not know how the data was partitioned in the [42]. Our result yields 0.9813 on the average accuracy on cross validation, and the highest and lowest cross validation accuracies are 0.9920 and 0.9733 respectively. Table 8 shows our average precision, recall, and F1-Score of five-fold cross validation on Yale's dataset. Table 7 shows confusion matrix for our classifier based on EfficientNet-B1. There were only 6 wrong predicted results, as shown in Figure 7. According to the comparison result on the same dataset, our proposed method outperforms the previous work done in [42] by yielding the higher accuracy. The overlapping cells were all correctly predicted in all five-fold cross validation which is quite obvious because the area of an overlapping cell is typically larger than other types of a single cell. Although accuracy gain using our model compared with the previous method is about 0.18% (7/3,737) which is not quite significant, but our model yield also better performance on both training and inference due to lots lower number of parameters.

VI. CONCLUSION & FUTURE WORKS

Herein, a simple method to segment RBCs is presented that has the ability to separate overlapping cells based on concave points, and classify RBCs into 12 classes. The process started from color normalization, which reduced the color space and allowed the trained model to not be biased on color. Next, contour extraction was used to extract the RBC contour from the background. Then, overlapping cells were separated using a new method to find concave points and use direct ellipse fitting to estimate the shape of a single RBC. Lastly, classification using EfficientNet-B1 showed the best result with augmentation. Moreover, further analysis for handling an imbalanced dataset revealed that weight balancing has the

TABLE 7. Confusion matrix for our proposed method on Yale's dataset

| Predicted Class | True Class | | | | | | | | | |
|-----------------|------------|------------|-------------|-------------|-------------|-------------|------------|-------------|------------|-----------|
| | Normal | Echinocyte | Dacrococyte | Schistocyte | Elliptocyte | Acanthocyte | Target | Stomatocyte | Spherocyte | Overlap |
| Normal | 203 | 0 | 0 | 0 | 0 | 0 | 0 | 0 | 0 | 0 |
| chinocyte | 0 | 63 | 0 | 0 | 0 | 0 | 0 | 0 | 0 | 0 |
| Dacrococyte | 0 | 0 | 16 | 1 | 1 | 0 | 0 | 0 | 0 | 0 |
| Schistocyte | 0 | 1 | 1 | 150 | 0 | 0 | 0 | 0 | 0 | 0 |
| Elliptocyte | 0 | 0 | 0 | 0 | 18 | 0 | 0 | 0 | 0 | 0 |
| Acanthocyte | 0 | 0 | 0 | 1 | 0 | 32 | 0 | 0 | 0 | 0 |
| Target cell | 0 | 0 | 0 | 0 | 0 | 0 | 145 | 0 | 0 | 0 |
| Stomatocyte | 0 | 0 | 0 | 0 | 0 | 0 | 0 | 22 | 0 | 0 |
| Spherocyte | 1 | 0 | 0 | 0 | 0 | 0 | 0 | 0 | 47 | 0 |
| Overlap | 0 | 0 | 0 | 0 | 0 | 0 | 0 | 0 | 0 | 46 |

TABLE 8. Average Precision, Recall, and F1-score of five-fold cross validation using our method on Yale's dataset

| RBC Types | Precision | Recall | F1-score |
|-------------|-----------|--------|----------|
| Normal | 0.995 | 0.985 | 0.990 |
| Echinocyte | 0.952 | 0.984 | 0.968 |
| Dacrococyte | 0.889 | 0.941 | 0.914 |
| Schistocyte | 0.974 | 0.949 | 0.961 |
| Elliptocyte | 0.889 | 0.941 | 0.914 |
| Acanthocyte | 0.848 | 0.933 | 0.889 |
| Target cell | 1.000 | 0.993 | 0.997 |
| Stomatocyte | 0.955 | 0.955 | 0.955 |
| Spherocyte | 0.958 | 0.958 | 0.958 |
| Overlap | 1.000 | 1.000 | 1.000 |

ability to reduce the bias of a trained model on the majority classes.

Many deep learning studies on RBCs still lack a standard public dataset to evaluate their performance. Our dataset has more samples and more types of RBCs than many previous studies, but it still requires to be improved for imbalanced problems. We plan to make this dataset publically available in the near future. For the method presented here, we used the EfficientNet model to classify the RBCs. However, the segmentation step is not a learning based method, which is a trend that has shown better results in many specific computer vision areas. Future work will evaluate the use of object detection methods to find a bounding box and classify the RBCs.

REFERENCES

- [1] J. Ford. Red blood cell morphology. *International Journal of Laboratory Hematology*, 35(3):351–357, 2013.
- [2] Mo Zhang, Xiang Li, Mengjia Xu, and Quanzheng Li. RBC Semantic Segmentation for Sickle Cell Disease Based on Deformable U-Net. In Alejandro F. Frangi, Julia A. Schnabel, Christos Davatzikos, Carlos Alberola-López, and Gabor Fichtinger, editors, *Medical Image Computing and Computer Assisted Intervention – MICCAI 2018*, Lecture Notes in Computer Science, pages 695–702, Cham, 2018. Springer International Publishing.
- [3] Annika Wong, Nantheera Anantrasirichai, Thanarat H. Chalidabhongse, Duangdao Palasuwan, Attakorn Palasuwan, and David Bull. Analysis of Vision-based Abnormal Red Blood Cell Classification. arXiv:2106.00389 [cs], June 2021.
- [4] Wei Qiu, Jiaming Guo, Xiang Li, Mengjia Xu, Mo Zhang, Ning Guo, and Quanzheng Li. Multi-label Detection and Classification of Red Blood Cells in Microscopic Images. arXiv:1910.02672 [cs, eess, stat], December 2019.
- [5] Ashkan Shakarami, Mohammad Bagher Menhaj, Ali Mahdavi-Hormat, and Hadis Tarrah. A fast and yet efficient YOLOv3 for blood cell detection. *Biomedical Signal Processing and Control*, 66:102495, April 2021.
- [6] Joseph Redmon and Ali Farhadi. Yolov3: An incremental improvement. CoRR, abs/1804.02767, 2018.
- [7] Mingxing Tan and Quoc V. Le. EfficientNet: Rethinking Model Scaling for Convolutional Neural Networks. arXiv:1905.11946 [cs, stat], September 2020.
- [8] Tsung-Yi Lin, Priya Goyal, Ross Girshick, Kaiming He, and Piotr Dollár. Focal Loss for Dense Object Detection. arXiv:1708.02002 [cs], February 2018.
- [9] Roopa B. Hegde, Keerthana Prasad, Harishchandra Hebbar, and I Sandhya. Peripheral blood smear analysis using image processing approach for diagnostic purposes: A review. *Biocybernetics and Biomedical Engineering*, 38(3):467–480, January 2018.
- [10] S. M. Mazalan, N. H. Mahmood, and M. A. A. Razak. Automated Red Blood Cells Counting in Peripheral Blood Smear Image Using Circular Hough Transform. In *Modelling and Simulation 2013 1st International Conference on Artificial Intelligence*, pages 320–324, December 2013.
- [11] Kitsuchart Pasupa, Supawit Vatathanavaro, and Suchat Tungjitnob. Convolutional neural networks based focal loss for class imbalance problem: a case study of canine red blood cells morphology classification. *Journal of Ambient Intelligence and Humanized Computing*, February 2020.
- [12] Ramin Soltanzadeh and Hossein Rabbani. Classification of three types of red blood cells in peripheral blood smear based on morphology. In *IEEE 10th INTERNATIONAL CONFERENCE ON SIGNAL PROCESSING PROCEEDINGS*, pages 707–710, October 2010.
- [13] S. Chandrasiri and P. Samarasinghe. Automatic anemia identification through morphological image processing. In *7th International Conference on Information and Automation for Sustainability*, pages 1–5, December 2014.
- [14] Razali Tomari, Wan Nurshazwani Wan Zakaria, Muhammad Mahadi Abdul Jamil, Faridah Mohd Nor, and Nik Farhan Nik Fuad. Computer Aided System for Red Blood Cell Classification in Blood Smear Image. *Procedia Computer Science*, 42:206–213, January 2014.
- [15] Howard Lee and Yi-Ping Phoebe Chen. Cell morphology based classification for red cells in blood smear images. *Pattern Recognition Letters*, 49:155–161, November 2014.
- [16] Miguel Romero-Rondón, Laura Sanabria-Rosas, Lola Bautista-Rozo, and Alfonso Mendoza. Algorithm for detection of overlapped red blood cells in microscopic images of blood smears. *Dyna (Medellin, Colombia)*, 83:188–195, September 2016.
- [17] I. Ahmad, S. N. H. S. Abdullah, and R. Z. Azma Raja Sabudin. Geometrical vs spatial features analysis of overlap red blood cell algorithm. In *2016 International Conference on Advances in Electrical, Electronic and Systems Engineering (ICAEEES)*, pages 246–251, November 2016.
- [18] Vasundhara Acharya and Preetham Kumar. Identification and red blood cell classification using computer aided system to diagnose blood disorders. In *2017 International Conference on Advances in Computing, Communications and Informatics (ICACCI)*, pages 2098–2104, September 2017.
- [19] Gopalakrishna Pillai Gopakumar, Murali Swetha, Gorthi Sai Siva, and Gorthi R. K. Sai Subrahmanyam. Convolutional neural network-based malaria diagnosis from focus stack of blood smear images acquired using custom-built slide scanner. *Journal of Biophotonics*, 11(3):e201700003, 2018.
- [20] Hajara Abdulkarim Aliyu, Mohd Azhar Abdul Razak, and Rubita

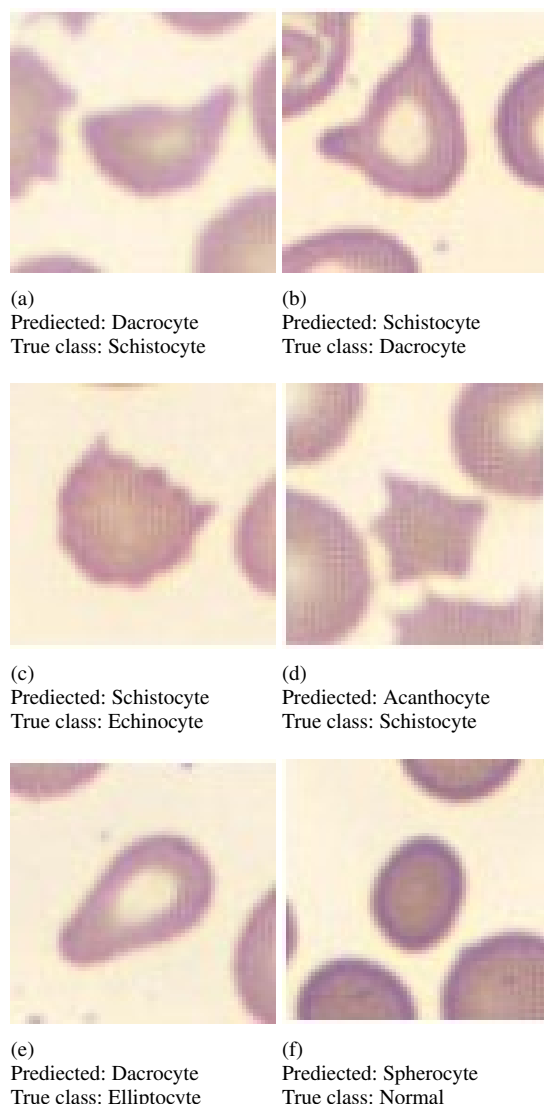


FIGURE 7. Among the 748 test images tested on EfficientNet-B1 using Yale's dataset, there were six misclassified images (a)-(f)

- Sudirman. Segmentation and detection of sickle cell red blood image. *AIP Conference Proceedings*, 2173(1):020004, November 2019.
- [21] Mamata Anil Parab and Ninad Dileep Mehendale. Red blood cell classification using image processing and CNN. *bioRxiv*, page 2020.05.16.087239, May 2020.
- [22] Virginia Mari E. Batitis, Merwin Jhan G. Caballes, Abigail A. Ciudad, Miccaela D. Diaz, Russel D. Flores, and Engr. Roselito E. Tolentin. Image Classification of Abnormal Red Blood Cells Using Decision Tree Algorithm. In *2020 Fourth International Conference on Computing Methodologies and Communication (ICCMC)*, pages 498–504, March 2020.
- [23] Laith Alzubaidi, Mohammed Fadhel, Omran Al-Shamma, and Jinglan Zhang. Robust and Efficient Approach to Diagnose Sickle Cell Anemia in Blood. pages 560–570. January 2020.
- [24] Pranati Rakshit and Kriti Bhowmik. Detection of Abnormal Findings in Human RBC in Diagnosing Sickle Cell Anaemia Using Image Processing. *Procedia Technology*, 10:28–36, January 2013.
- [25] Nicola Ritter and James Cooper. Segmentation and Border Identification of Cells in Images of Peripheral Blood Smear Slides. In *Proceedings of the Thirtieth Australasian Conference on Computer Science - Volume 62, ACSC '07*, pages 161–169, Darlinghurst, Australia, Australia, 2007. Australian Computer Society, Inc.
- [26] S. Kareem, R. C. S. Morling, and I. Kale. A novel method to count the red blood cells in thin blood films. In *2011 IEEE International Symposium of Circuits and Systems (ISCAS)*, pages 1021–1024, May 2011.
- [27] Mehdi Habibzadeh, A. Krzyzak, Thomas Fevens, and Ali Sadr. Counting of RBCs and WBCs in noisy normal blood smear microscopic images. volume 7963, March 2011.
- [28] V. Sharma, A. Rathore, and G. Vyas. Detection of sickle cell anaemia and thalassaemia causing abnormalities in thin smear of human blood sample using image processing. In *2016 International Conference on Inventive Computation Technologies (ICICT)*, volume 3, pages 1–5, August 2016.
- [29] R. Cai, Q. Wu, R. Zhang, L. Fan, and C. Ruan. Red blood cell segmentation using Active Appearance Model. In *2012 IEEE 11th International Conference on Signal Processing*, volume 3, pages 1641–1644, October 2012.
- [30] Hanung Adi Nugroho, Son Ali Akbar, and E. Elsa Herdiana Murhandarwati. Feature extraction and classification for detection malaria parasites in thin blood smear. In *2015 2nd International Conference on Information Technology, Computer, and Electrical Engineering (ICITACEE)*, pages 197–201, October 2015.
- [31] Dyah Aruming Tyas, Tri Ratnaningsih, Agus Harjoko, and Sri Hartati. The Classification of Abnormal Red Blood Cell on The Minor Thalassaemia Case Using Artificial Neural Network and Convolutional Neural Network. In *Proceedings of the International Conference on Video and Image Processing, ICVIP 2017*, pages 228–233, New York, NY, USA, 2017. ACM.
- [32] Maria Delgado-Ortet, Angel Molina-Borrás, Santiago Alférez, José Rodelar, and Anna Merino. A Deep Learning Approach for Segmentation of Red Blood Cell Images and Malaria Detection. *Entropy*, 22:657, June 2020.
- [33] A. Sadafi, M. Radolko, I. Serafeimidis, and S. Hadlak. Red Blood Cells Segmentation: A Fully Convolutional Network Approach. In *2018 IEEE Intl Conf on Parallel Distributed Processing with Applications, Ubiquitous Computing Communications, Big Data Cloud Computing, Social Computing Networking, Sustainable Computing Communications (ISPA/IUCC/BDCloud/SocialCom/SustainCom)*, pages 911–914, December 2018.
- [34] Kevin de Haan, Hatice Ceylan Koydemir, Yair Rivenson, Derek Tseng, Elizabeth Van Dyne, Lissette Bakic, Doruk Karınca, Kyle Liang, Megha Ilango, Esin Gumustekin, and Aydogan Ozcan. Automated screening of sickle cells using a smartphone-based microscope and deep learning. *npj Digital Medicine*, 3(1):1–9, May 2020.
- [35] Mo Zhang, Xiang Li, Mengjia Xu, and Quanzheng Li. Image Segmentation and Classification for Sickle Cell Disease using Deformable U-Net. arXiv:1710.08149 [cs, q-bio], October 2017.
- [36] Mengjia Xu, Dimitrios P. Papageorgiou, Sabia Z. Abidi, Ming Dao, Hong Zhao, and George Em Karniadakis. A deep convolutional neural network for classification of red blood cells in sickle cell anemia. *PLOS Computational Biology*, 13(10):e1005746, 2017.
- [37] M. González-Hidalgo, F. A. Guerrero-Peña, S. Herold-García, A. Jaume-i Capó, and P. D. Marrero-Fernández. Red Blood Cell Cluster Separation From Digital Images for Use in Sickle Cell Disease. *IEEE Journal of Biomedical and Health Informatics*, 19(4):1514–1525, July 2015.
- [38] Samiur Rahman, Bakht Azam, Sana Ullah Khan, Muhammad Awais, Ishfaq Ali, and Raja Jalees ul Hussen Khan. Automatic identification of abnormal blood smear images using color and morphology variation of RBCs and central pallor. *Computerized Medical Imaging and Graphics*, 87:101813, January 2021.
- [39] Adnan Khashman. IBCIS: Intelligent blood cell identification system. *Progress in Natural Science*, 18(10):1309–1314, October 2008.
- [40] Sagar Yeruva, M. Sharada Varalakshmi, B. Pavan Gowtham, Y. Hari Chandana, and PESN Krishna Prasad. Identification of Sickle Cell Anemia Using Deep Neural Networks. *Emerging Science Journal*, 5(2):200–210, April 2021.
- [41] Z. Liang, A. Powell, I. Ersoy, M. Poostchi, K. Silamut, K. Palaniappan, P. Guo, M. A. Hossain, A. Sameer, R. J. Maude, J. X. Huang, S. Jaeger, and G. Thoma. CNN-based image analysis for malaria diagnosis. In *2016 IEEE International Conference on Bioinformatics and Biomedicine (BIBM)*, pages 493–496, December 2016.
- [42] Thomas J. S. Durant, Eben M. Olson, Wade L. Schulz, and Richard Torres. Very Deep Convolutional Neural Networks for Morphologic Classification of Erythrocytes. *Clinical Chemistry*, 63(12):1847–1855, December 2017.
- [43] M. Z. Alom, C. Yakopcic, T. M. Taha, and V. K. Asari. Microscopic Blood Cell Classification Using Inception Recurrent Residual Convolutional

- Neural Networks. In NAECON 2018 - IEEE National Aerospace and Electronics Conference, pages 222–227, July 2018.
- [44] Prayag Tiwari, Jia Qian, Qiuchi Li, Benyou Wang, Deepak Gupta, Ashish Khanna, Joel J. P. C. Rodrigues, and Victor Hugo C. de Albuquerque. Detection of subtype blood cells using deep learning. *Cognitive Systems Research*, 52:1036–1044, December 2018.
- [45] Laith Alzubaidi, Mohammed A. Fadhel, Omran Al-Shamma, Jinglan Zhang, and Ye Duan. Deep Learning Models for Classification of Red Blood Cells in Microscopy Images to Aid in Sickle Cell Anemia Diagnosis. *Electronics*, 9(3):427, March 2020.
- [46] H. Abdulkarim, M. A. A. Razak, R. Sudirman, and N. Ramli. A deep learning AlexNet model for classification of red blood cells in sickle cell anemia. 2020.
- [47] Justin M. Johnson and Taghi M. Khoshgoftaar. Survey on deep learning with class imbalance. *Journal of Big Data*, 6(1):1–54, December 2019.
- [48] A. Fitzgibbon, M. Pilu, and R.B. Fisher. Direct least square fitting of ellipses. *IEEE Transactions on Pattern Analysis and Machine Intelligence*, 21(5):476–480, May 1999.
- [49] Aw Fitzgibbon and Rb Fisher. A Buyer's Guide to Conic Fitting. In *Proceedings of the British Machine Vision Conference 1995*, pages 51.1–51.10. British Machine Vision Association, 1995.
- [50] Gao Huang, Zhuang Liu, Laurens van der Maaten, and Kilian Q. Weinberger. Densely Connected Convolutional Networks. *arXiv:1608.06993 [cs]*, January 2018.



KORRANAT NARUENATTHANASET received the B.E. degree in computer engineering in 2017. Since 2018, he has been a master student under the supervision of Prof. Chalidabhongse. In summer 2019, he spent a month internship under Prof. Anantrasirichai's supervision. His current research interests include medical imaging, image classification, and deep learning for computer vision.



THANARAT H. CHALIDABHONGSE received her B.Eng. degree in Computer Engineering from Chulalongkorn University, M.S. in Computer Science from the University of Southern California, and Ph.D. in Computer Science from the University of Maryland, College Park. Currently, she works as a full-time faculty member of the Department of Computer Engineering at Chulalongkorn University, where she has done many researches in her expertise including image and video processing, human motion understanding, object detection and recognition, scene text analysis, medical imaging, and real-time vision. Her statistical background subtraction method has been one of the highly regarded methods in computer vision research community.



DUANGDAO PALASUWAN received her B.E. degree in Medical Technology from Naresuan University, and Ph.D. in Tropical Medicine from Mahidol University, Thailand. Currently, she works as a full-time faculty member of the Department of Clinical Microscopy at Chulalongkorn University. Her research interest includes fundamental study of red blood cell disorders, pathophysiology of severe malaria, and flow cytometry.



NANTHEERA ANANTRASIRICHA (S'04–M'07) received the B.E. degree in Electrical Engineering from Chulalongkorn University, Bangkok, Thailand, in 2000, and the Ph.D. degree in electrical and electronic engineering from the University of Bristol, Bristol, U.K., in 2007.

She is currently a Senior Research Fellow with the Visual Information Laboratory, University of Bristol. Her current research interests include image and video coding, image analysis and enhancement, image fusion, medical imaging, texture-based image analysis, and remote sensing.



ATTAKORN PALASUWAN received his B.Sc. degree in Medical Technology and M.Sc. Biotechnology from Chulalongkorn University, Thailand, and received Docteur en Science from Université de Nice Sophia Antipolis, France. He is an Associate Professor of Department of Clinical Microscopy, Faculty of Allied Health Sciences, Chulalongkorn University. Currently, he is a PhD Program Chair of Clinical Hematology Sciences, Chulalongkorn University. His research interest includes the innovation using clinical microscopic imaging and real-time vision for medical laboratory learning & clinical laboratory diagnosis.

...